



Contents lists available at ScienceDirect

Journal of Biomechanics

journal homepage: www.elsevier.com/locate/jbiomech
www.JBiomech.com

Short communication

Automated and objective removal of bifurcation aneurysms: Incremental improvements, and validation against healthy controls



Aslak W. Bergersen^a, Christophe Chnafa^b, Diego Gallo^c, Marina Piccinelli^d, David A. Steinman^b, Kristian Valen-Sendstad^{a,*}

^a Department of Computational Physiology, Simula Research Laboratory, Lysaker, Norway

^b Department of Mechanical and Industrial Engineering, University of Toronto, Toronto, ON, Canada

^c Department of Mechanical and Aerospace Engineering, Politecnico di Torino, Torino, Italy

^d Department of Radiology and Imaging Sciences, Emory University, GA, USA

ARTICLE INFO

Article history:

Accepted 11 September 2019

Keywords:

Mechanobiology
Wall shear stress
Wall shear stress gradients
Aneurysm pathogenesis
Subarachnoid hemorrhage

ABSTRACT

Abnormal hemodynamic stresses are thought to correlate with aneurysm initiation, growth, and rupture. We have previously investigated the role of wall shear stress (WSS) and WSS gradients (WSSG) in search for a mechanistic link to formation of sidewall aneurysms using an automated and objective tool for aneurysm removal and arterial reconstruction in combination with computational fluid dynamics (CFD). However, we warned against the use of the tool for bifurcation type aneurysms because of a potential unrealistic reconstruction of the apex. We hypothesized that inclusion of additional morphological features from the surrounding vasculature could overcome these constraints. We extended the previously published method for removal and reconstruction of the bifurcation vasculature based on diverging and converging points of the parent and daughter artery centerlines, to also include two new centerlines between the daughter vessels, one of them passed through the bifurcation center. Validation was performed by comparing the efficacy of the two algorithms, using ten healthy models of the internal carotid artery terminus as ground truth. Qualitative results showed that the bifurcation apices became smoother relative to the original algorithm; more consistent with the reference models. This was reflected quantitatively by a reduced maximum distance between the reference and reconstructed surfaces, although not statistically significant. Furthermore, the modified algorithm also quantitatively improved CFD derived WSS and WSSG, especially the latter. In conclusion, the modified algorithm does not perfectly reconstruct the bifurcation apex, but provides an incremental improvement, especially important for the derived hemodynamic metrics of interest in vascular pathobiology.

© 2019 Elsevier Ltd. All rights reserved.

1. Introduction

Rupture of an intracranial aneurysm is the most common cause of subarachnoid hemorrhage (Wiebers et al., 2003). The vast majority of aneurysms are asymptomatic and incidentally detected when patients undergo neuroimaging for unrelated reasons. However, risk of clinical intervention can exceed the natural risk of rupture, which is as low as 1% annually (Rinkel et al., 1998) making optimal patient-specific treatment decisions difficult. Morphological indices have historically been used clinically for risk of rupture stratification (Raghavan et al., 2005), but aneurysm morphology and size are ultimately surrogates for hemodynamically induced wall shear stress (WSS) that contribute to vessel wall adaption,

remodeling, and vascular pathogenesis (Malek et al., 1999; Morbiducci et al., 2016). Medical image-based computational fluid dynamics (CFD) (Taylor and Steinman, 2010) has been extensively used in the investigation of vascular pathology, e.g., retrospectively correlating flow phenotypes and stresses with aneurysm rupture status in search for prospective clinical use (Xiang et al., 2011; Cebral et al., 2011).

However, 'predicting' aneurysm rupture status in large databases with a retrospectively known clinical outcome can be problematic for a number of reasons. Aneurysm rupture is an event that may change both morphology and size (Schneiders et al., 2014; Skodvin et al., 2017), only certain aneurysms have endothelial cells (Frösen et al., 2004), and the aneurysm wall has a different structure compared to healthy arteries (Canham et al., 1999). Additionally, there are uncertainties related to modeling of aneurysm flows, like neck size overestimation with 3D rotational angiography

* Corresponding author.

E-mail address: kvs@simula.no (K. Valen-Sendstad).

(Schneiders et al., 2013), image segmentation, which is both laborious and operator-dependent (Valen-Sendstad et al., 2018), and numerical solution strategies (Valen-Sendstad and Steinman, 2014; Khan et al., 2015). Therefore, studying the fundamental role of hemodynamics in aneurysms might be more intricate than originally anticipated. However, since the same stimuli (WSS/WSSG) are believed to be involved in aneurysm initiation (Gao et al., 2008; Kulcsár et al., 2011), growth (Sugiyama et al., 2012; Francis et al., 2013), and rupture (Cebal et al., 2005; Xiang et al., 2011), one can investigate the hemodynamic stimulus and vascular response before aneurysms have formed, without the aforementioned limitations. Hence, studying aneurysm initiation can provide mechanistic links that are paramount for understanding fundamental vascular remodeling.

Ford et al. (Ford et al., 2009) developed a tool for objective aneurysm removal and arterial reconstruction for investigating the plausible hemodynamic stimulus prior to sidewall aneurysm formation. They also warned about the application to bifurcation aneurysms, and clearly stated that the tool 'remains to be verified'. The latter is difficult because medical images of the pre-aneurysmal vasculature are rarely available. Secondly, the high-resolution contrast-based computed tomography images needed to adequately reconstruct a bifurcation apex, can naturally not be obtained from healthy individuals to limit potentially harmful radiation (Hendee and O'Connor, 2012). From previous usage of the tool developed by Ford et al., for instance applied to sidewall aneurysms Valen-Sendstad et al. (2014) we hypothesized that

the bifurcation apex was occasionally reconstructed with an artificial "notch" at the apex. We, therefore, proposed a technical improvement to the original algorithm. We also acquired access to segmentation of intracranial blood vessels in ten patients that underwent neurointensive care where no vascular abnormalities were found, which enabled validation. The latter is indeed the only possible solution since the vasculature is unknown in the presence of an aneurysm, which the algorithm actually is independent of. The aim of the study was to reconstruct an artificially removed bifurcation, and compare the results of the two reconstruction algorithms to the reference and *a priori* known bifurcation surface, especially focusing on relevant CFD derived stresses. In the following, we will refer to the bifurcation surfaces as *reference*, *Ford*, and *modified* corresponding to the unmodified healthy surface, the reconstructed surface from Ford et al., and our modified algorithm, respectively.

2. Methods

2.1. Parent artery and bifurcation reconstruction

We acquired access to 3D angiograms from ten patients that underwent neurointensive care where no vascular abnormalities were found, originally collected for the open-source Aneurisk database, and subsequently made publicly available (Aneurisk-Team, 2012). Fig. 1 is adapted from Ford et al. and outlines the algorithm for intracranial aneurysm removal and parent artery

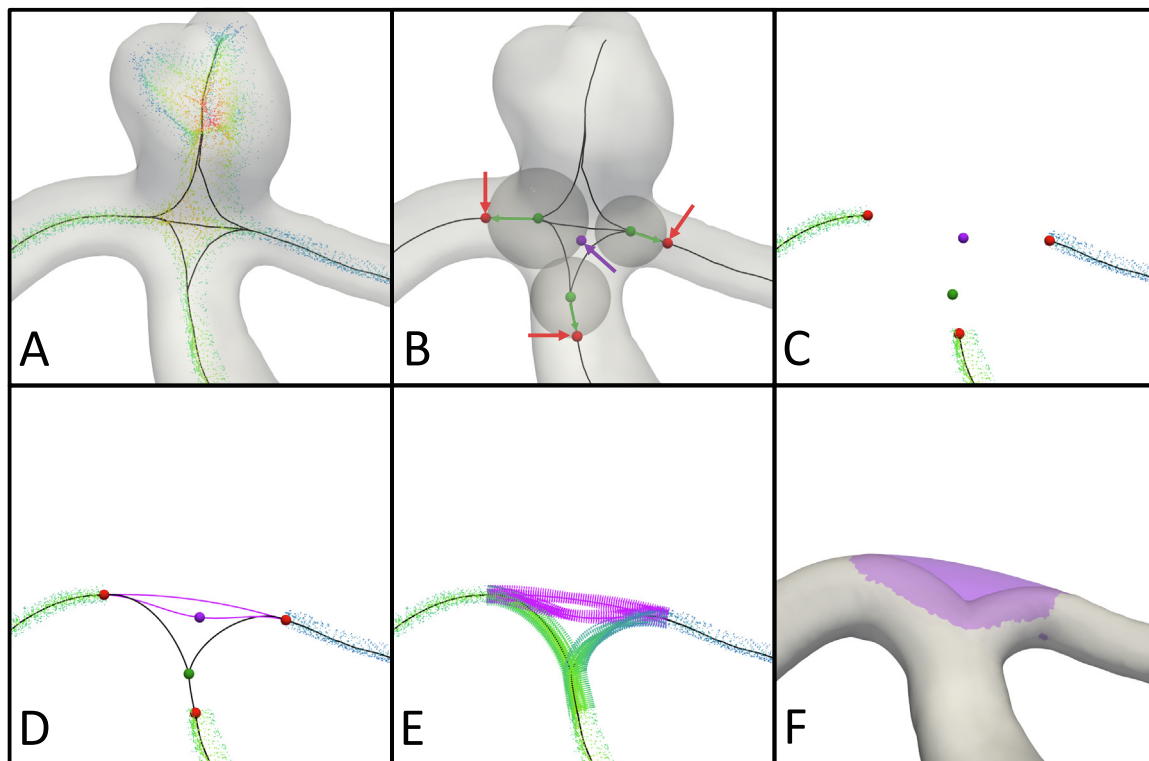


Fig. 1. Illustration of the algorithm for removing a bifurcation aneurysm. The additions to the algorithm, relative to Ford et al., is highlighted in purple. Note that to ease comparison with Ford et al. we here illustrate the algorithm on the same model, but for the remainder of the paper we are applying the algorithm to bifurcations without aneurysms for validation purposes. **Step A**, compute the Voronoi diagram and five centerlines; two from the parent artery to each daughter branch, two from each daughter branch to the aneurysm sac, and one between the two daughter branches. **Step B**, the green dots are located where the centerlines coordinates diverge; referred to as diverging points, and the arithmetic mean of the coordinates of these is defined as the bifurcation center location, shown in purple. The diverging points are then moved one radius of the local minimal inscribed sphere away from the bifurcation center along the centerlines, as indicated by the green arrows; now referred to as clipping points. **Step C**, subtract the centerlines and Voronoi diagram that are located in between the clipping points. **Step D**, create a total of four new centerlines, two of which are passed through the diverging point from the parent artery to the daughter branches using third order splines. The remaining two start and end at the daughter branches, where one of them is passed through the bifurcation center. **Step E**, extrapolate the old Voronoi diagram along the new centerlines. **Step F**, envelope the Voronoi diagram to create a new surface. (For interpretation of the references to colour in this figure legend, the reader is referred to the web version of this article.)

reconstruction. Note that we here illustrate the algorithm using the same model as in Ford et al., but that we here apply the algorithm to models without aneurysms only. Briefly, the algorithm is based on manipulating the Voronoi diagram, which is an alternative representation of a surface (Piccinelli et al., 2009), and associated centerlines, to both remove and reconstruct the bifurcation. Details are provided in the caption of Fig. 1. The main difference between the original and the modified algorithm is that the Voronoi diagram is interpolated onto two new centerlines between the daughter vessels, these changes are colored purple in Fig. 1.

2.2. CFD, wall shear stress, and wall shear stress gradients

CFD simulations were performed to investigate the effects of the reconstruction algorithms on hemodynamic stresses. The Vascular Modelling ToolKit (Antiga et al., 2008) was used to extend the inlet and outlets five times the local radius, and create meshes that on average consisted of three million tetrahedron cells with four boundary layers, previously demonstrated to be sufficient to resolve WSS (Khan et al., 2015). Pulsatile CFD simulations were performed assuming blood to behave as a Newtonian fluid (Khan et al., 2017) using the Oasis solver (Mortensen and Valen-Sendstad, 2015), designed to obtain a solution that preserves kinetic energy while minimizing numerical dispersion and diffusion errors, taking 10,000 time steps per cycle with a period of 0.951s using an older adult waveform (Hoi et al., 2010). We specified a fully developed Womersley velocity profile at the inlet and a time-averaged cross-sectional mean velocity of 0.27 m/s (Valen-Sendstad et al., 2015) with a flow splitting approach for the out-flow boundary as detailed in (Chnafa et al., 2018).

The efficacy of the reconstruction algorithms was quantified with respect to the mean and maximum distance, curvature, WSS, and WSSG; measured relatively to the reference surface or

associated CFD simulations. All metrics were computed along the intersection between the objectively defined bifurcation plane (Piccinelli et al., 2011) and surface, see white lines in Fig. 3A, now referred to as *bifurcation lines*. To quantitatively measure the differences, we sampled WSS and WSSG along the normalized bifurcation line, and used a spline representation to compute the maximum curvature, a metric describing the bifurcation apex “notch”. A one-sided paired t-test was used to check if the modified method performed significantly better, setting the level of significance to p -value < 0.05, not adjusting for multiple tests.

3. Results

3.1. Parent artery and bifurcation reconstruction

Fig. 2 shows models 1–5 of the reference surface in white with the results of the original and modified surface reconstruction algorithms colored in red in sub-plots A and B, respectively, all in opaque. We have zoomed into model 1 to better highlight the differences. These qualitative results arguably show that the modified algorithm produce reconstructed surfaces closer to the reference surface, most importantly at the apex of the bifurcation. That is, the modified algorithm does not produce the same artificial “notch”, especially apparent in the models 1, 2, 4, and 5 shown in Fig. 2A. The remaining five models are shown in the Appendix with broadly consistent results.

3.2. Hemodynamic metrics: Wall shear stress and wall shear stress gradients

Focusing now on qualitative CFD derived results, Fig. 3A shows bifurcation WSS maps obtained on the modified, reference, and Ford surfaces, respectively. The WSS maps show largely similar

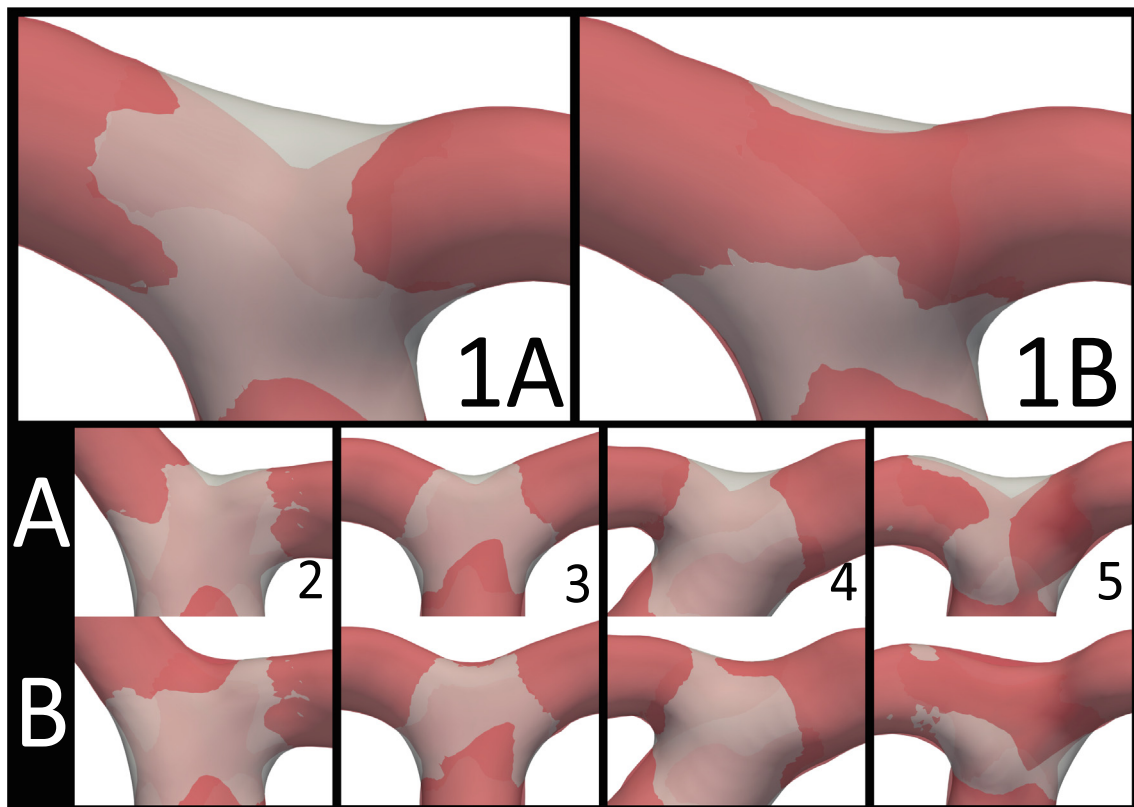


Fig. 2. The figure shows the reference surface in opaque, with the results from the original and modified surface reconstruction algorithms colored in red in sub-plots A and B, respectively. (For interpretation of the references to colour in this figure legend, the reader is referred to the web version of this article.)

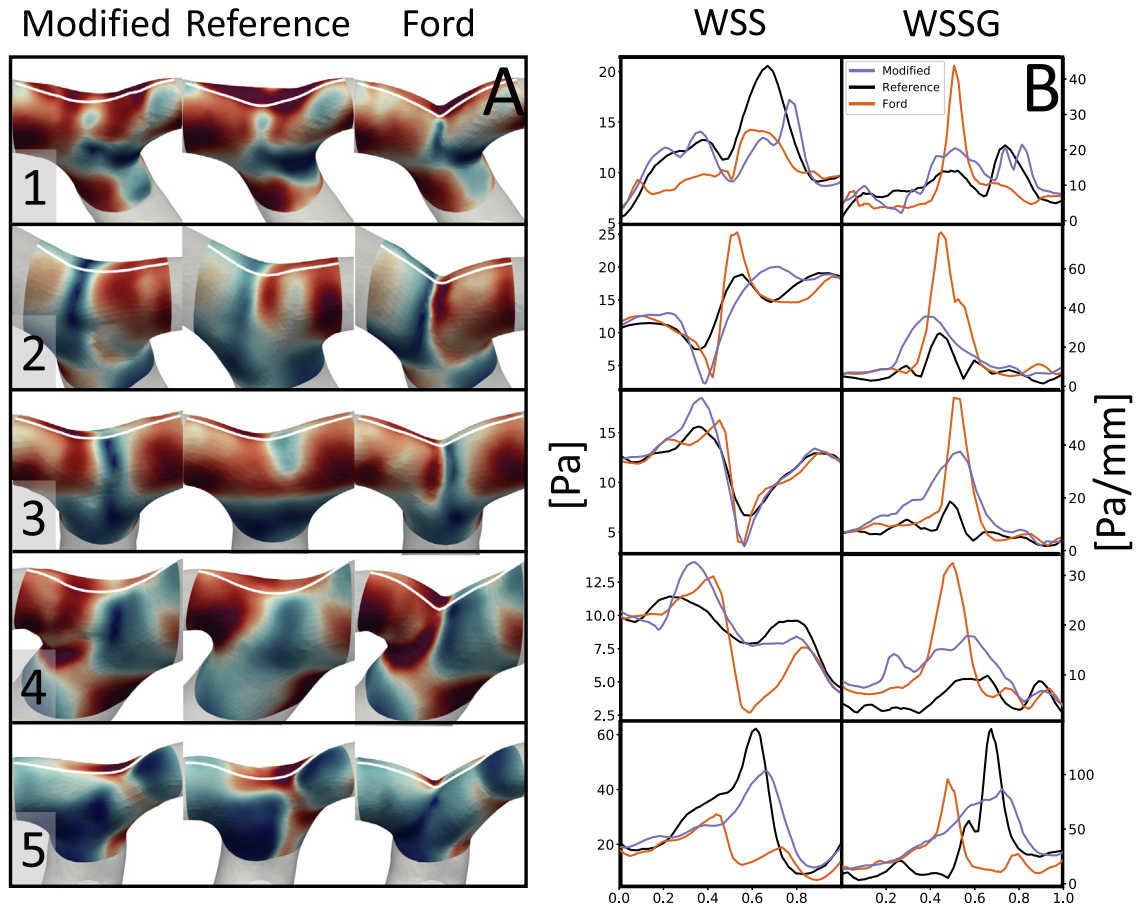


Fig. 3. **A** Wall shear stress (WSS) maps from computational fluid dynamic simulations of the modified, reference, and Ford models, from left to right, respectively, and bifurcation lines shown in white. The absolute values of the WSS are indicated in the panel to the right. **B** WSS and WSS gradients along the bifurcation lines where the colors black, orange, and blue refers to the modified, reference, and Ford models, respectively. (For interpretation of the references to colour in this figure legend, the reader is referred to the web version of this article.)

global trends, but with clearly visible differences at the bifurcation apex. This is further highlighted by the corresponding WSS and WSSG values along the bifurcation lines shown in Fig. 3B; especially WSSG is overestimated by the original algorithm. The remaining five models are shown in the Appendix with broadly consistent result.

Table 1 shows quantitative results and demonstrates that both the curvature, WSS, and WSSG were significantly closer to the reference values, with *p-values* < 0.05 marked in bold. The maximum

distance between the reference and reconstructed surfaces was also reduced with the modified algorithm, although not statistically significant.

4. Discussion

We have shown that a minor modification of Ford et al.'s algorithm can reconstruct arterial bifurcations that are more consistent with the reference bifurcation obtained from state-of-the-art med-

Table 1

The table shows quantitative result based on the error measurements between the reference surface versus those obtained from the original and modified algorithms, respectively. *p-values* below 0.05 % are marked in bold.

Metric	Measure	Mean absolute error (SD)		<i>p-value</i>
		Ford	Modified	
Distance [mm]	Average	0.06 (0.03)	0.06 (0.04)	0.408
	Max	0.30 (0.15)	0.19 (0.11)	0.076
Curvature [$\frac{1}{\text{mm}}$]	Max	2.03 (0.48)	0.24 (0.26)	<0.001
WSS [Pa]	Average	7.27 (11.02)	5.63 (8.73)	0.037
	Max	17.57 (22.33)	12.90 (16.66)	0.081
WSSG [Pa/mm]	Average	12.54 (8.23)	9.41 (5.49)	0.012
	Max	50.22 (29.40)	26.82 (17.47)	0.001

ical images. As a result, the computed WSS and WSSG from the reconstructed surfaces are statistically and phenotypically improved compared to the original algorithm. Since the vast majority of aneurysms are located in bifurcations, the modified algorithm could increase the number of subjects, increase the rigor of aneurysm initiation research, and accelerate our understanding of fundamental vascular pathobiology. The latter can ultimately contribute to further advances in research on aneurysm risk of rupture.

We have previously shown that there is relatively high intra- and interlaboratory uncertainty in segmentation of intracranial arteries (Valen-Sendstad et al., 2018). To reduce the uncertainty in the segmentation we chose to focus on the ICA terminus since it is the largest intracranial artery, and is therefore the least sensitive to segmentation errors because of the high voxel-to-vessel ratio. However, we have also compared the geometrical metrics of middle- and anterior cerebral artery bifurcations and obtained equivalent results for the maximum curvature (average absolute errors of 2.09 and 0.52 [$\frac{1}{mm}$] using the Ford and modified algorithm, respectively, p -value < 0.001). These results, however, are associated with higher uncertainties due to the smaller voxel-to-vessel ratio. Hence, a limitation is that validation has just been performed on ten models. Another “feature” associated with the current methods is namely that neither algorithms were designed or capable to reproduce a proximal stenosis, as observed in model 7, see Fig. 5 of the Appendix. Both algorithms produced a too wide arterial segment at the stenosis location, which resulted in a lowered WSS/WSSG, relative to the reference model. The quantitative results are admittedly sensitive to the bifurcation plane, as is obvious from Figs. 3 and 5, however, they are objectively defined (Piccinelli et al., 2011).

Relative to previous studies, our WSS/WSSG figures/lines appear to be noisier since we used human “patient-specific” models instead of idealized (Kono et al., 2013; Lauric et al., 2018) or animal models (Meng et al., 2010). We do not consider this a limitation, but rather a result of controlling numerical viscosity, and the use of potentially “irregular” human models from the Aneurysm database. Smoothing the surfaces is indeed possible, but we consider the current approach the most sensitive, and consequently the most rigorous one.

Although we have shown that the modified algorithm better reconstructs the bifurcation, it still remains to quote Ford et al., namely that users must still “exercise their judgment if a particular

case is a good candidate for similar studies”. The code and associated tutorials are provided online, see <https://github.com/KVSlab/morphMan>, which also includes other methods for objectively altering additional morphological features of anatomically plausible vascular geometries.

5. Conclusion

We have shown that an incremental modification of Ford et al.’s aneurysm removal tools plausibly give better agreement with the reference surface and the corresponding stresses on the arterial wall. The modified algorithm can accelerate and broaden research on the hemodynamic stresses associated with aneurysm initiation, with the ultimate extrapolation to rupture prediction.

Declaration of Competing Interest

The authors have no conflicts of interest to declare.

Acknowledgment

The study was supported by The Research Council of Norway through a Center of Excellence grant to the Center for Biomedical Computing at Simula Research Laboratory, project number 179578. This work was also carried out as a part of the Centre for Cardiological Innovation, and SIMMIS, project number 262827, funded by the Research Council of Norway. Computations were performed on the GPC supercomputer at the SciNet (Loken et al., 2010) HPC Consortium. SciNet is funded by: the Canada Foundation for Innovation under the auspices of Compute Canada; the Government of Ontario; Ontario Research Fund - Research Excellence; and the University of Toronto. Post processing was performed on the Abel Cluster, owned by the University of Oslo and the Norwegian metacenter for High Performance Computing (NOTUR), and operated by the Department for Research Computing at USIT, the University of Oslo IT-department, Grant No. nn9316k.

Appendix

See Figs. 4 and 5.

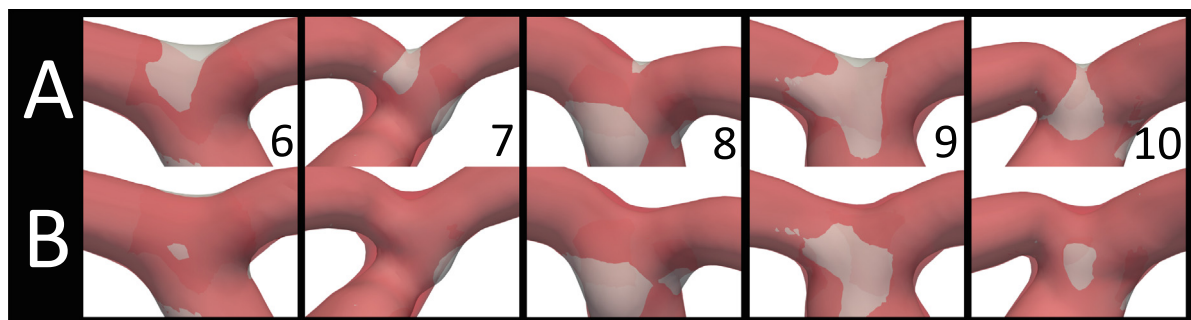


Fig. 4. The figure shows the reference surface in opaque, with the results of the original and modified surface reconstruction algorithms colored in red in sub-plots A and B, respectively.

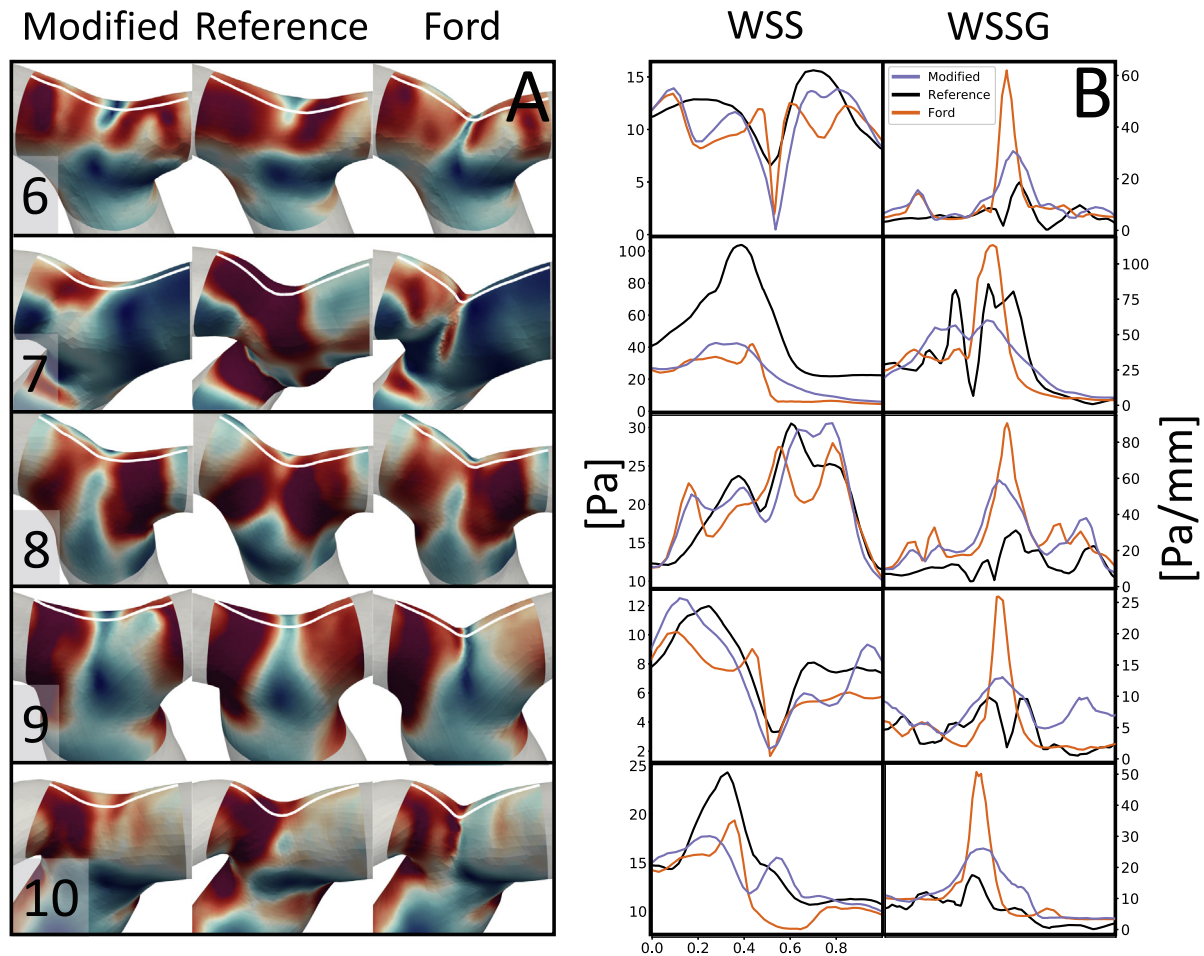


Fig. 5. **A** Wall shear stress (WSS) maps from computational fluid dynamic simulations of the modified, reference, and Ford models, from left to right, respectively, and bifurcation lines shown in white. The absolute values of the WSS are indicated in the panel to the right. **B** WSS and WSSG along the bifurcation lines where the colors black, orange, and blue refers to the modified, reference, and Ford models, respectively. (For interpretation of the references to colour in this figure legend, the reader is referred to the web version of this article.)

References

- Aneurisk-Team, 2012. AneuriskWeb project website, <http://ecm2.mathcs.emory.edu/aneuriskweb>. Web Site, accessed 01.08.2018.
- Antiga, L., Piccinelli, M., Botti, L., Ene-Iordache, B., Remuzzi, A., Steinman, D.A., 2008. An image-based modeling framework for patient-specific computational hemodynamics. *Med. Biol. Eng. Comput.* 46 (11), 1097–1112.
- Canham, P.B., Finlay, H.M., Kiernan, J.A., Ferguson, G.G., 1999. Layered structure of saccular aneurysms assessed by collagen birefringence. *Neurol. Res.* 21 (7), 618–626.
- Cebral, J.R., Castro, M.A., Burgess, J.E., Pergolizzi, R.S., Sheridan, M.J., Putman, C.M., 2005. Characterization of cerebral aneurysms for assessing risk of rupture by using patient-specific computational hemodynamics models. *Am. J. Neuroradiol.* 26 (10), 2550–2559.
- Cebral, J.R., Mut, F., Weir, J., Putman, C., 2011. Quantitative characterization of the hemodynamic environment in ruptured and unruptured brain aneurysms. *Am. J. Neuroradiol.* 32 (1), 145–151.
- Chnafa, C., Brina, O., Pereira, V., Steinman, D., 2018. Better than nothing: a rational approach for minimizing the impact of outflow strategy on cerebrovascular simulations. *Am. J. Neuroradiol.* 39 (2), 337–343.
- Ford, M.D., Hoi, Y., Piccinelli, M., Antiga, L., Steinman, D.A., 2009. An objective approach to digital removal of saccular aneurysms: technique and applications. *British J. Radiol.* 82 (Special Issue), S55–S61.
- Francis, S.E., Tu, J., Qian, Y., Avolio, A.P., 2013. A combination of genetic, molecular and haemodynamic risk factors contributes to the formation, enlargement and rupture of brain aneurysms. *J. Clin. Neurosci.* 20 (7), 912–918.
- Frösen, J., Piippo, A., Paetau, A., Kangasniemi, M., Niemelä, M., Hernesniemi, J., Jääskeläinen, J., 2004. Remodeling of saccular cerebral artery aneurysm wall is associated with rupture: histological analysis of 24 unruptured and 42 ruptured cases. *Stroke* 35 (10), 2287–2293.
- Gao, L., Hoi, Y., Swartz, D.D., Kolega, J., Siddiqui, A., Meng, H., 2008. Nascent aneurysm formation at the basilar terminus induced by hemodynamics. *Stroke* 39 (7), 2085–2090.
- Hendee, W.R., O'Connor, M.K., 2012. Radiation risks of medical imaging: separating fact from fantasy. *Radiology* 264 (2), 312–321.
- Hoi, Y., Wasserman, B.A., Xie, Y.J., Najjar, S.S., Ferruci, L., Lakatta, E.G., Gerstenblith, G., Steinman, D.A., 2010. Characterization of volumetric flow rate waveforms at the carotid bifurcations of older adults. *Physiol. Meas.* 31 (3), 291.
- Khan, M., Steinman, D.A., Valen-Sendstad, K., 2017. Non-Newtonian versus numerical rheology: Practical impact of shear-thinning on the prediction of stable and unstable flows in intracranial aneurysms. *Int. J. Num. Methods Biomed. Eng.* 33 (7), e2836.
- Khan, M., Valen-Sendstad, K., Steinman, D., 2015. Narrowing the expertise gap for predicting intracranial aneurysm hemodynamics: impact of solver numerics versus mesh and time-step resolution. *Am. J. Neuroradiol.* 36 (7), 1310–1316.
- Kono, K., Masuo, O., Nakao, N., Meng, H., 2013. De novo cerebral aneurysm formation associated with proximal stenosis. *Neurosurgery* 76 (6), E1080–E1090.
- Kulcsár, Z., Ugron, A., Marosfői, M., Berentei, Z., Paál, G., Szikora, I., 2011. Hemodynamics of cerebral aneurysm initiation: the role of wall shear stress and spatial wall shear stress gradient. *Am. J. Neuroradiol.* 32 (3), 587–594.
- Lauric, A., Greim-Kuczewski, K., Antonov, A., Dardik, G., Magida, J.K., Hippelheuser, J.E., Kono, K., Malek, A.M., 2018. Proximal parent vessel tapering is associated with aneurysm at the middle cerebral artery bifurcation. *Neurosurgery*.
- Loken, C., Gruner, D., Groer, L., Peltier, R., Bunn, N., Craig, M., Henriques, T., Dempsey, J., Yu, C.-H., Chen, J., et al., 2010. SciNet: lessons learned from building a power-efficient top-20 system and data centre. In: *Journal of Physics: Conference Series*. vol. 256(1). IOP Publishing, p. 012026.
- Malek, A.M., Alper, S., Izumo, S., 1999. Hemodynamic shear stress and its role in atherosclerosis. *JAMA* 282 (21), 2035–2042.
- Meng, H., Natarajan, S., Gao, L., Ionita, C., Kolega, J., Siddiqui, A., Mocco, J., 2010. Aneurysmal changes at the basilar terminus in the rabbit elastase aneurysm model. *Am. J. Neuroradiol.* 31 (3), E35–E36.
- Morbiducci, U., Kok, A.M., Kwak, B.R., Stone, P.H., Steinman, D.A., Wentzel, J.J., et al., 2016. Atherosclerosis at arterial bifurcations: evidence for the role of haemodynamics and geometry. *Thrombosis Haemost.* 115 (3), 484–492.

- Mortensen, M., Valen-Sendstad, K., 2015. Oasis: A high-level/high-performance open source Navier-Stokes solver. *Comput. Phys. Commun.* 188, 177–188.
- Piccinelli, M., Bacigaluppi, S., Boccardi, E., Ene-Iordache, B., Remuzzi, A., Veneziani, A., Antiga, L., 2011. Geometry of the internal carotid artery and recurrent patterns in location, orientation, and rupture status of lateral aneurysms: an image-based computational study. *Neurosurgery* 68 (5), 1270–1285.
- Piccinelli, M., Veneziani, A., Steinman, D.A., Remuzzi, A., Antiga, L., 2009. A framework for geometric analysis of vascular structures: application to cerebral aneurysms. *IEEE Trans. Med. Imaging* 28 (8), 1141–1155.
- Raghavan, M.L., Ma, B., Harbaugh, R.E., 2005. Quantified aneurysm shape and rupture risk. *J. Neurosurg.* 102 (2), 355–362.
- Rinkel, G.J.E., Djibuti, M., Algra, A., van Gijn, J., 1998. Prevalence and risk of rupture of intracranial aneurysms: a systematic review. *Stroke* 29 (1), 251–256.
- Schneiders, J., Marquering, H., Antiga, L., Van den Berg, R., VanBavel, E., Majoie, C., 2013. Intracranial aneurysm neck size overestimation with 3D rotational angiography: the impact on intra-aneurysmal hemodynamics simulated with computational fluid dynamics. *Am. J. Neuroradiol.* 34 (1), 121–128.
- Schneiders, J., Marquering, H., van den Berg, R., VanBavel, E., Velthuis, B., Rinkel, G., Majoie, C., 2014. Rupture-associated changes of cerebral aneurysm geometry: high-resolution 3d imaging before and after rupture. *Am. J. Neuroradiol.* 35 (7), 1358–1362.
- Skodvin, T.Ø., Johnsen, L.-H., Gjertsen, Ø., Isaksen, J.G., Sorteberg, A., 2017. Cerebral aneurysm morphology before and after rupture: nationwide case series of 29 aneurysms. *Stroke* 48 (4), 880–886.
- Sugiyama, S.-I., Meng, H., Funamoto, K., Inoue, T., Fujimura, M., Nakayama, T., Omodaka, S., Shimizu, H., Takahashi, A., Tominaga, T., 2012. Hemodynamic analysis of growing intracranial aneurysms arising from a posterior inferior cerebellar artery. *World Neurosurgery* 78 (5), 462–468.
- Taylor, C.A., Steinman, D.A., 2010. Image-based modeling of blood flow and vessel wall dynamics: applications, methods and future directions. *Ann. Biomed. Eng.* 38 (3), 1188–1203.
- Valen-Sendstad, K., Bergersen, A.W., Shimogonya, Y., Goubergrits, L., Bruening, J., Pallares, J., Cito, S., Piskin, S., Pekkan, K., Geers, A.J., et al., 2018. Real-world variability in the prediction of intracranial aneurysm wall shear stress: the 2015 International Aneurysm CFD Challenge. *Cardiovascular Eng. Technol.*, 1–21.
- Valen-Sendstad, K., Piccinelli, M., KrishnankuttyRema, R., Steinman, D.A., 2015. Estimation of inlet flow rates for image-based aneurysm CFD models: where and how to begin? *Ann. Biomed. Eng.* 43 (6), 1422–1431.
- Valen-Sendstad, K., Piccinelli, M., Steinman, D.A., 2014. High-resolution computational fluid dynamics detects flow instabilities in the carotid siphon: Implications for aneurysm initiation and rupture? *J. Biomech.* 47 (12), 3210–3216.
- Valen-Sendstad, K., Steinman, D.A., 2014. Mind the gap: impact of Computational Fluid Dynamics solution strategy on prediction of intracranial aneurysm hemodynamics and rupture status indicators. *Am. J. Neuroradiol.* 35 (3), 536–543.
- Wiebers et al., 2003. Unruptured intracranial aneurysms: natural history, clinical outcome, and risks of surgical and endovascular treatment. *Lancet* 362 (9378), 103–110.
- Xiang, J., Natarajan, S.K., Tremmel, M., Ma, D., Mocco, J., Hopkins, L.N., Siddiqui, A.H., Levy, E.L., Meng, H., 2011. Hemodynamic-morphologic discriminants for intracranial aneurysm rupture. *Stroke* 42 (1), 144–152.